Scientific Research Publishing

American Journal of Computational Mathematics, 2026, 16(2), 27-43
https://www.scirp.org/journal/ajcm
ISSN Online: 2161-1211
ISSN Print: 2161-1203

Computational Analysis of MHD Mixed Convection in a Heated Lid-Driven Cavity with Fins

Rezaul Haque[1], Abdul Alim[2], Laek Sazzad Andallah[1], Shahidul Alam[3]*

[1]Department of Mathematics, Jahangirnagar University (JU), Dhaka, Bangladesh
[2]Department of Mathematics, Bangladesh University of Engineering and Technology (BUET), Dhaka, Bangladesh
[3]Department of EEE, Dhaka International University (DIU), Dhaka, Bangladesh
Email: rezaul.controller.butex@gmail.com, a0alim@gmail.com, andallah@juniv.edu, *shdlalam@gmail.com

How to cite this paper: Haque, R., Alim, A., Andallah, L.S. and Alam, S. (2026) Computational Analysis of MHD Mixed Convection in a Heated Lid-Driven Cavity with Fins. *American Journal of Computational Mathematics*, **16**, 27-43.
https://doi.org/10.4236/ajcm.2026.162003

Received: March 28, 2026
Accepted: May 9, 2026
Published: May 12, 2026

Abstract

A numerical investigation of magnetohydrodynamic (MHD) mixed convection in a lid-driven square cavity with internal heat generation is presented. The cavity is filled with an electrically conducting fluid, and the top wall moves at a constant velocity while the remaining walls are stationary. A uniform magnetic field is applied parallel to the lid motion. The governing continuity, momentum, and energy equations are solved using the Galerkin weighted residual method, finite element method under the Boussinesq approximation. The effects of the Richardson number, Hartmann number, Prandtl number, and internal heat generation parameter on flow and heat transfer characteristics are examined. Results are provided in terms of streamlines, isotherms, the average Nusselt number within the cavity, and the local Nusselt number along the horizontal line of the cavity, depending on the various combinations of the dimensionless governing parameters. The results indicate that increasing *Ha* suppresses fluid motion and reduces convective heat transfer, whereas higher *Ri* enhances buoyancy-driven flow. Internal heat generation elevates temperature levels and reduces the overall heat transfer rate. The study highlights the competing roles of magnetic damping and buoyancy forces in controlling thermal performance.

Keywords

Mixed Convection, MHD, Lid-Driven Cavity, Finite Element Method, Heat Generation

1. Introduction

Mixed convection in lid-driven cavities has attracted significant attention due to

its wide applicability in thermal engineering systems such as heat exchangers, cooling of electronic devices, and energy storage units. The complex interaction between shear-driven flow induced by the moving lid and buoyancy-driven flow due to temperature gradients governs the overall heat transfer characteristics. Early investigations primarily focused on simple square enclosures with differentially heated walls, establishing fundamental insights into flow behavior and heat transfer mechanisms [1].

With the advancement of computational techniques, researchers extended these studies to include magnetohydrodynamic (MHD) effects. The application of an external magnetic field introduces a Lorentz force that suppresses fluid motion and alters thermal transport. Rahman and Alim [2] analyzed MHD mixed convection in a lid-driven cavity with internal heating elements and reported that increasing the Hartmann number significantly dampens fluid circulation and reduces the Nusselt number. Similar findings were reported by Jani *et al.* [3] and Hussein *et al.* [4], who demonstrated that magnetic fields can effectively control convective flow structures in various enclosure geometries.

Subsequent studies incorporated internal heat sources and geometric modifications to enhance heat transfer performance. Rabbi *et al.* [5] investigated ferrofluid-filled cavities and showed that heater configuration plays a crucial role in determining thermal efficiency. Alam *et al.* [6]-[8] examined sinusoidal walls and partially heated boundaries, revealing that non-uniform thermal conditions significantly influence vortex formation and temperature distribution. Munshi *et al.* [9] further explored non-standard cavity geometries and highlighted the role of corner heaters in modifying flow patterns.

The influence of entropy generation and thermodynamic irreversibility in MHD mixed convection systems was studied by Chamkha *et al.* [10], who emphasized the importance of electrical conductivity models. Later, Chowdhury and Alim [11] and Haque *et al.* [12] investigated complex configurations involving wavy walls and multiple heated blocks, reporting enhanced heat transfer due to increased surface area and flow interaction. Similarly, Fayz-Al-Asad *et al.* [13] and Bakar *et al.* [14] analyzed the effects of fins and internal heat generation, demonstrating that such modifications can significantly improve thermal performance depending on their placement and intensity.

Recent research trends have focused on advanced working fluids and configurations. Farahani *et al.* [15] examined nanofluid flow under magnetic fields and porous media effects, while Runa *et al.* [16] studied semi-circular enclosures with internal obstacles using finite element methods. Keya *et al.* [17] explored heat exchangers embedded within lid-driven cavities, highlighting their practical engineering relevance. More recently, Mahmuda Maya *et al.* [18] and Ali *et al.* [19] investigated MHD mixed convection using nanofluids and hybrid nanofluids, demonstrating improved heat transfer performance compared to conventional fluids.

Furthermore, Sarker and Alam [20] and Theeb *et al.* [21] extended these analyses to complex geometries and hybrid nanofluid systems under magnetic influ-

ence, emphasizing the combined effects of internal heat sources, cavity shape, and fluid properties. These studies collectively indicate that incorporating internal structures such as fins and obstacles can enhance heat transfer by increasing the effective heat transfer area and promoting fluid mixing.

Despite these extensive investigations, limited attention has been given to the combined effects of lid-driven motion, MHD influence, internal heating, and fin-based augmentation within a single computational framework. In particular, the role of fins in modifying flow structure and heat transfer under magnetic fields remains inadequately explored. Therefore, a comprehensive computational study focusing on MHD mixed convection in a heated lid-driven cavity with fins is essential to bridge this research gap and provide deeper insights into optimizing thermal system performance.

Assumptions:

1) Laminar, incompressible, Newtonian fluid flow.

2) 2D square cavity (x, y directions).

3) Uniform internal heat generation Q.

4) Constant physical properties ($\rho, \mu, k, \beta, \sigma$).

5) Magnetic field applied, negligible induced magnetic field (low magnetic Reynolds number).

6) Boussinesq approximation: density variations only affect buoyancy term.

2. Geometric Model and Mathematical Formulation

A two-dimensional square cavity is considered in the present investigation, as schematically illustrated in **Figure 1**. The upper wall of the cavity moves horizontally in its own plane with a constant velocity U_0, while the remaining walls satisfy the no-slip boundary condition. The thermal boundary conditions are imposed such that the left vertical and bottom walls are maintained at a uniform high temperature T_h, whereas the right vertical wall is kept at a constant low temperature T_c. The upper moving wall is assumed to be thermally insulated. The cavity comprises six solid fins, with three affixed to the left vertical wall and the remaining three to the right vertical wall at equal spacing. All fins are assumed to be thermally insulated and have a length l and width b.

The fluid inside the cavity is electrically conducting, and all cavity walls are assumed to be electrically insulating. A uniform magnetic field of constant strength B_0 is applied parallel to the direction of the lid motion. The induced magnetic field generated by the fluid motion is assumed to be negligible in comparison with the applied magnetic field, thereby decoupling the Navier–Stokes equations from Maxwell's equations.

The thermo-physical properties of the fluid are assumed to be constant, except for the density variation in the buoyancy term, which is modeled using the Boussinesq approximation. Viscous dissipation effects are neglected. The fluid is further assumed to be Newtonian, incompressible, and the flow is considered to be steady and laminar.

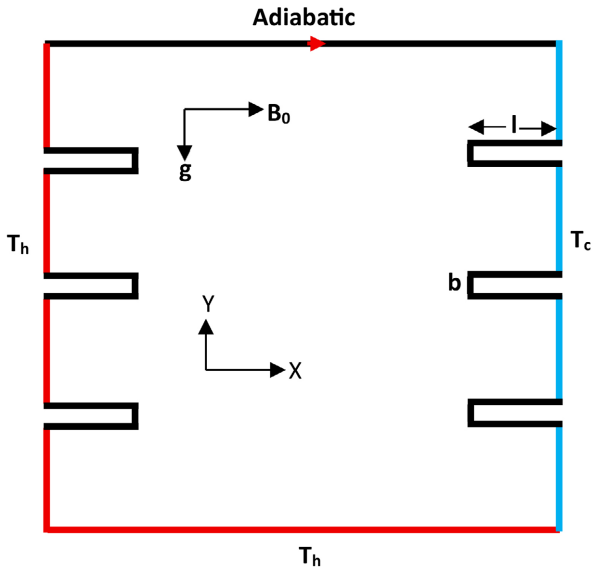

Figure 1. Schematic diagram of the physical model with six inside fins along the vertical walls.

Continuity Equation:
$$\frac{\partial u}{\partial x}+\frac{\partial v}{\partial y}=0 \tag{1}$$

Momentum Equations (Navier-Stokes with MHD and buoyancy)

***x*-momentum:**
$$\rho\left(u\frac{\partial u}{\partial x}+v\frac{\partial u}{\partial y}\right)=-\frac{\partial p}{\partial x}+\mu\left(\frac{\partial^2 u}{\partial x^2}+\frac{\partial^2 u}{\partial y^2}\right)+\sigma B^2 u \tag{2}$$

***y*-momentum:**
$$\rho\left(u\frac{\partial v}{\partial x}+v\frac{\partial v}{\partial y}\right)=-\frac{\partial p}{\partial y}+\mu\left(\frac{\partial^2 v}{\partial x^2}+\frac{\partial^2 v}{\partial y^2}\right)+\rho g\beta\left(T-T_c\right)+\sigma B^2 v \tag{3}$$

where:

- u,v = velocity components in x and y.
- p = pressure.
- μ = dynamic viscosity.
- ρ = density.
- σ = electrical conductivity.
- B = magnetic field strength.
- β = thermal expansion coefficient.
- g = gravity acceleration.
- T = temperature.

The MHD Lorentz force term is usually $-\sigma B^2 u$ for the x-direction, but depending on orientation of the magnetic field, it can appear in both x and y directions.

Energy Equation:
$$\rho c_p\left(u\frac{\partial T}{\partial x}+v\frac{\partial T}{\partial y}\right)=k\left(\frac{\partial^2 T}{\partial x^2}+\frac{\partial^2 T}{\partial y^2}\right)+Q \tag{4}$$

where:

- k = thermal conductivity.
- c_p = specific heat at constant pressure.
- Q = volumetric internal heat generation.

Boundary Conditions:

Wall	Velocity Condition	Thermal Condition
Left ($x = 0$)	$u = 0,\ v = 0$	$T = T_h$ (hot)
Right ($x = L$)	$u = 0,\ v = 0$	$T = T_c$ (cold)
Top ($y = L$)	$u = U_0,\ v = 0$	$\partial T/\partial y = 0$ (adiabatic)
Bottom ($y = 0$)	$u = 0,\ v = 0$	$T = T_h$ (hot)

Dimensionless Formulation:
Introduce dimensionless variables:

$$X = \frac{x}{L}, Y = \frac{y}{L}, U = \frac{u}{U_0}, V = \frac{v}{U_0}, \theta = \frac{T - T_c}{T_h - T_c}, P = \frac{p}{\rho U_0^2}$$

Dimensionless equations:

Continuity:
$$\frac{\partial U}{\partial X} + \frac{\partial V}{\partial Y} = 0 \tag{5}$$

x-momentum:
$$U\frac{\partial U}{\partial X} + V\frac{\partial U}{\partial Y} = -\frac{\partial P}{\partial X} + \frac{1}{Re}\left(\frac{\partial^2 U}{\partial X^2} + \frac{\partial^2 U}{\partial Y^2}\right) - \frac{Ha^2}{Re}U \tag{6}$$

y-momentum:
$$U\frac{\partial V}{\partial X} + V\frac{\partial V}{\partial Y} = -\frac{\partial P}{\partial Y} + \frac{1}{Re}\left(\frac{\partial^2 V}{\partial X^2} + \frac{\partial^2 V}{\partial Y^2}\right) + \frac{Gr}{Re^2}\theta - \frac{Ha^2}{Re}V \tag{7}$$

Energy:
$$U\frac{\partial \theta}{\partial X} + V\frac{\partial \theta}{\partial Y} = \frac{1}{Re\,Pr}\left(\frac{\partial^2 \theta}{\partial X^2} + \frac{\partial^2 \theta}{\partial Y^2}\right) + \frac{Q^*}{Re\,Pr} \tag{8}$$

Dimensionless numbers:

1) Reynolds number: $Re = \dfrac{U_0 L}{\nu}$

2) Prandtl number: $Pr = \dfrac{\nu}{\alpha} = \dfrac{\mu c_p}{k}$

3) Grashof number: $Gr = \dfrac{g\beta\left(T_h - T_c\right)L^3}{\nu^2}$

4) Hartmann number: $Ha = BL\sqrt{\dfrac{\sigma}{\mu}}$

5) Internal heat generation parameter: $Q^* = \dfrac{QL^2}{k\left(T_h - T_c\right)}$

Dimensionless Boundary Conditions:

Wall	Velocity Condition	Thermal Condition
Left ($X = 0$)	$U = 0,\ V = 0$	$\theta = 1$
Right ($X = L$)	$U = 0,\ V = 0$	$\theta = 0$

Continued

Top ($Y = L$)	$U = U_0,\ V = 0$	$\partial\theta/\partial Y = 0$ (adiabatic)
Bottom ($Y = 0$)	$U = 0,\ V = 0$	$\partial\theta/\partial Y = 1$

Since the convective heat transfer coefficient: h and Nusselt number Nu, depend on the temperature gradient at a flat surface, $\left(-\frac{\partial T}{\partial n}\right)$ where n is normal direction to the ∂n surface.

Therefore, we can obtain the rate of heat flux from each of the walls. The corresponding average Nusselt number at the heated surface is defined as:

$$Nu_{av} = \int_0^1 Nu\mathrm{d}x$$

where Re, Pr, Gr, Ha and Q^* are denote Reynold number, Prandtl number, Hartmann number, Grashof number and heat generation coefficient respectively.

3. Numerical Method

The dimensionless governing equations describing the magnetohydrodynamic (MHD) mixed convection flow with internal heat generation in a lid-driven square cavity, together with the corresponding boundary conditions, are solved numerically using the Galerkin weighted residual finite element method (FEM). The theoretical formulation and numerical implementation of this method are based on the standard procedures reported by Taylor and Hood and Dechaumphai.

The physical domain is discretized into a finite number of uniformly distributed quadrilateral elements using a mapped mesh technique. Within each element, the dependent variables—namely velocity components, temperature, and pressure—are approximated by appropriate interpolation (shape) functions. The Galerkin approach is then employed to derive the weak form of the nonlinear governing equations by selecting the weighting functions identical to the interpolation functions. The resulting integral equations are evaluated numerically using Gaussian quadrature, leading to a system of coupled nonlinear algebraic equations. The prescribed boundary conditions, including the lid-driven velocity, thermal conditions on the cavity walls, and magnetic field effects, are incorporated directly into the algebraic system. To solve the nonlinear system, the equations are linearized using the Newton–Raphson iterative technique. At each iteration, the resulting linearized system is solved using the Triangular Factorization method, which ensures computational efficiency and numerical stability.

The iterative solution process is continued until the following convergence criterion is satisfied for all dependent variables:

$$\max\left|\phi^{n+1} - \phi^{n}\right| \le 10^{-6},$$

where ϕ represents the dimensionless velocity components, temperature, and pressure, and n denotes the iteration level.

To ensure the accuracy and reliability of the numerical solutions, a grid independence test is performed using progressively refined meshes. The final computational mesh is selected such that further refinement produces negligible changes in the key flow and thermal characteristics. Additionally, the numerical results are validated by comparison with previously published benchmark solutions available in the literature, showing excellent agreement.

4. Grid Sensitivity Test and Mesh Generation

In order to obtain grid independent solution, a grid refinement study is performed for a square cavity with 6 fins while $Pr = 0.71$, $Ha = 50$ and $Ri = 6$. Figure 2 illustrates the convergence of the average Nusselt number (Nu) at the heated surface as the grid is refined. It can be observed that grid independence is achieved at 15,956 elements, beyond which any further increase in the number of elements results in only minimal changes to Nu, as shown in Table 1. For the grid refinement tests, six different non-uniform grids were evaluated with varying numbers of nodes and elements: 1213 nodes and 2464 elements; 1778 nodes and 3452 elements; 2489 nodes and 4852 elements; 3698 nodes and 7364 elements; 7986 nodes and 15,956 elements; 27,334 nodes and 54,680 elements. Based on these results, the grid with 7986 nodes and 15,956 elements is suitable for achieving an optimal balance between accuracy and computational efficiency in the simulation.

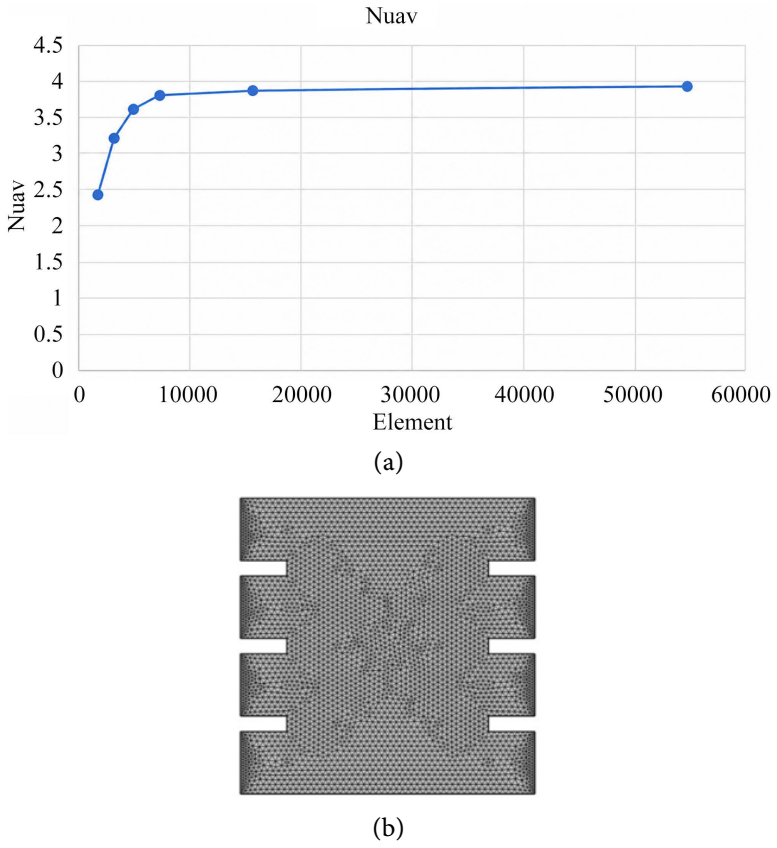

Figure 2. (a) Grid sensitivity test. (b) Mesh configuration of the cavity with fins.

Table 1. Nu_{av} at different mesh system.

Node	1213	1778	2489	3698	7986	27,334
Element	2464	3452	4852	7364	15,956	54,680
Nu	2.4297	3.2839	3.6642	3.8465	3.8920	3.9273

5. Code Validation

The validation of the numerical code was carried out by comparing streamlines, isotherms, and the vertical velocity component along the horizontal centerline of the cavity with the results presented in **Figures 3-5**. As observed from these figures, the present results show good agreement with the reference data, confirming the accuracy and reliability of the numerical model.

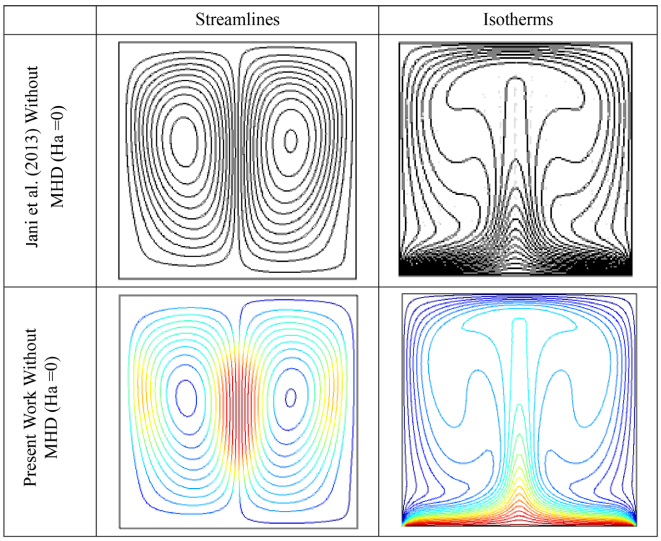

Figure 3. Code validation for $Ra = 10^5$ and $Pr = 0.71$

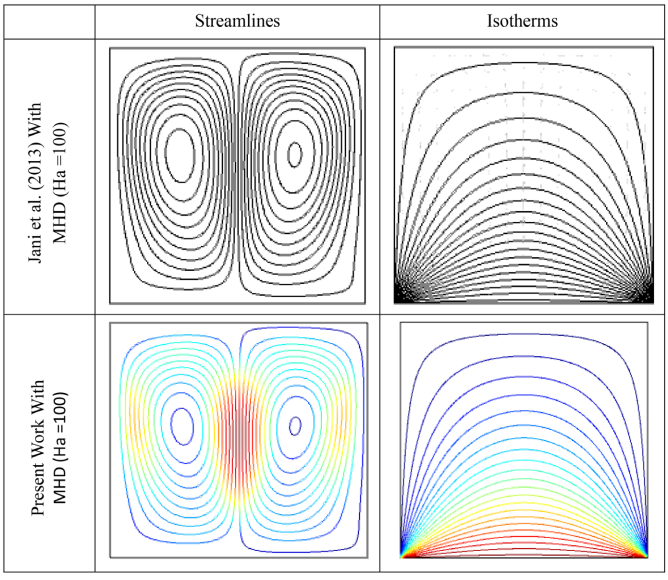

Figure 4. Code validation for $Ra = 10^5$ and $Pr = 0.71$.

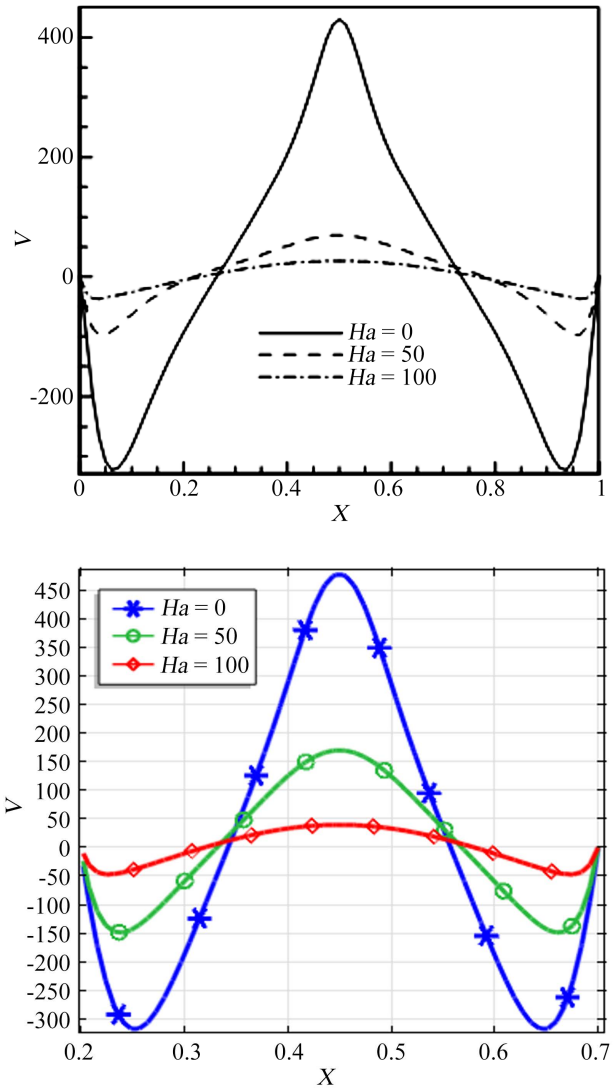

Figure 5. Code validation for vertical velocity component along the horizontal central line of the cavity with Hartmann number at $Ra = 10^5$ and $Pr = 0.71$.

6. Results and Discussion

The numerical results obtained from the present finite element simulations are analyzed to elucidate the effects of the Richardson number (Ri), Hartmann number (Ha), and internal heat generation (Q^*) on the flow structure and thermal behavior within the lid-driven cavity. The discussion is supported by streamline contours, isotherm distributions, velocity and temperature profiles, and local Nusselt number variations.

6.1. Effect of Richardson Number (Ri)

Figures 6-9 illustrate the influence of the Richardson number ($Ri = 0.3$, 3, 6, and 9) on flow and thermal fields at fixed parameters ($Ha = 50$, $Re = 2000$, $Pr = 0.71$). The Richardson number represents the relative strength of buoyancy-driven natural convection to shear-driven forced convection.

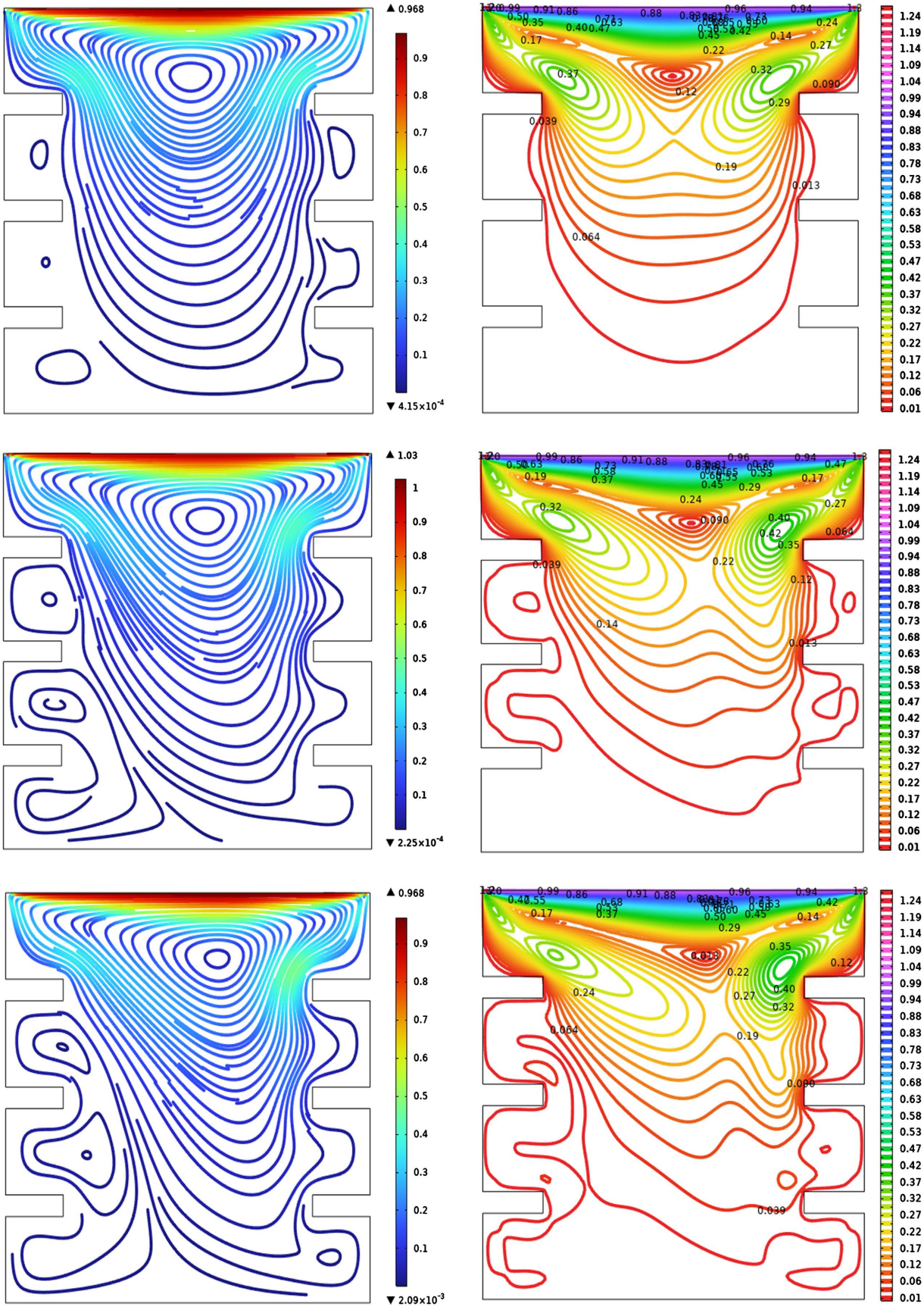
▲ 0.968
0.9
0.8
0.7
0.6
0.5
0.4
0.3
0.2
0.1
▼ 4.15×10^-4
1.24
1.19
1.14
1.09
1.04
0.99
0.94
0.88
0.83
0.78
0.73
0.68
0.63
0.58
0.53
0.47
0.42
0.37
0.32
0.27
0.22
0.17
0.12
0.06
0.01
▲ 1.03
1
0.9
0.8
0.7
0.6
0.5
0.4
0.3
0.2
0.1
▼ 2.25×10^-4
▲ 0.968
0.9
0.8
0.7
0.6
0.5
0.4
0.3
0.2
0.1
▼ 2.09×10^-3

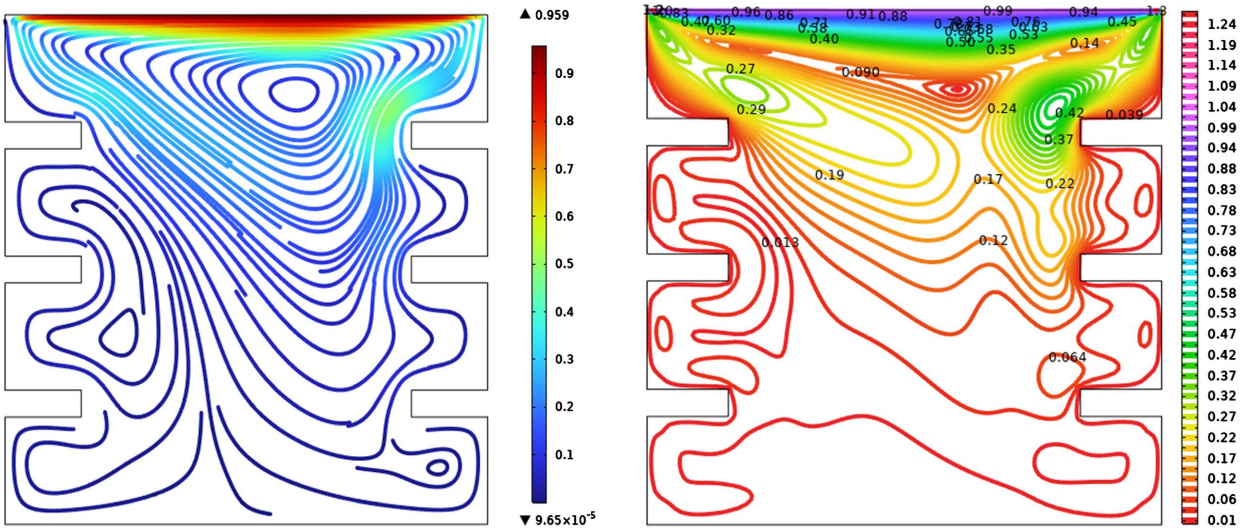

Figure 6. Streamlines (left column); Isotherms (right column) for $Ri = 0.3, 3, 6, 9$ while $Ha = 50$, $Pr = 0.71$ and $Re = 2000$.

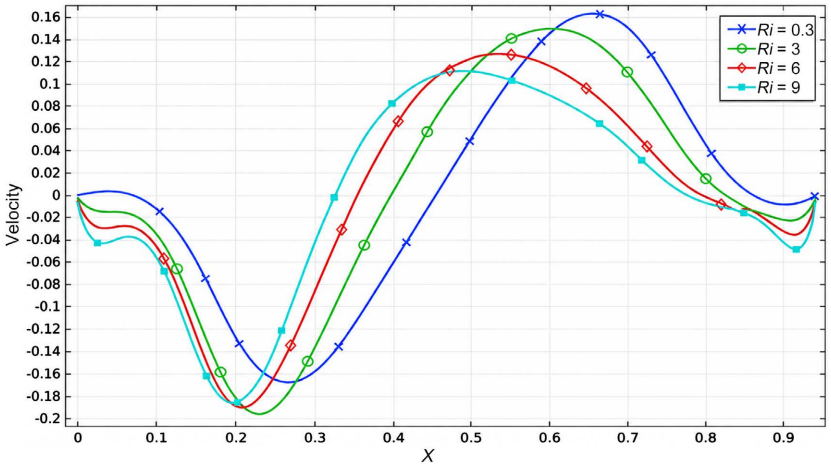

Figure 7. Effect of Velocity profile for Ri along the line $y = 0.6$, while $Ha = 50$, $Pr = 0.71$ and $Re = 2000$.

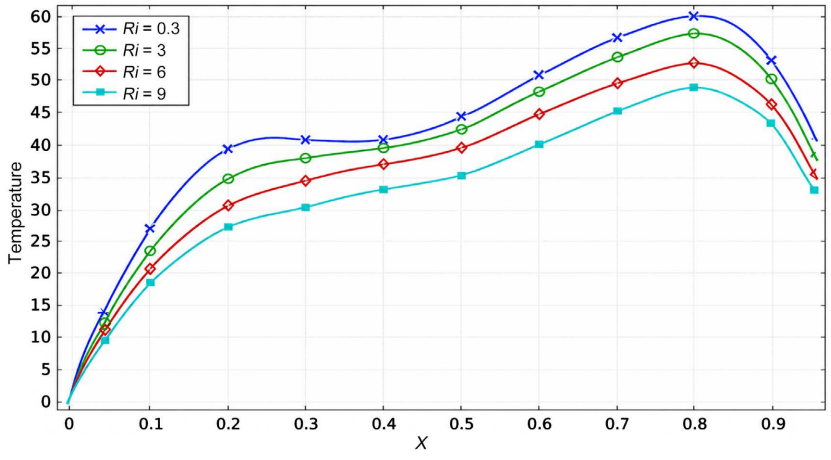

Figure 8. Effect of Temperature profile for Ri along the line $y = 0.6$, while $Ha = 50$, $Pr = 0.71$ and $Re = 2000$.

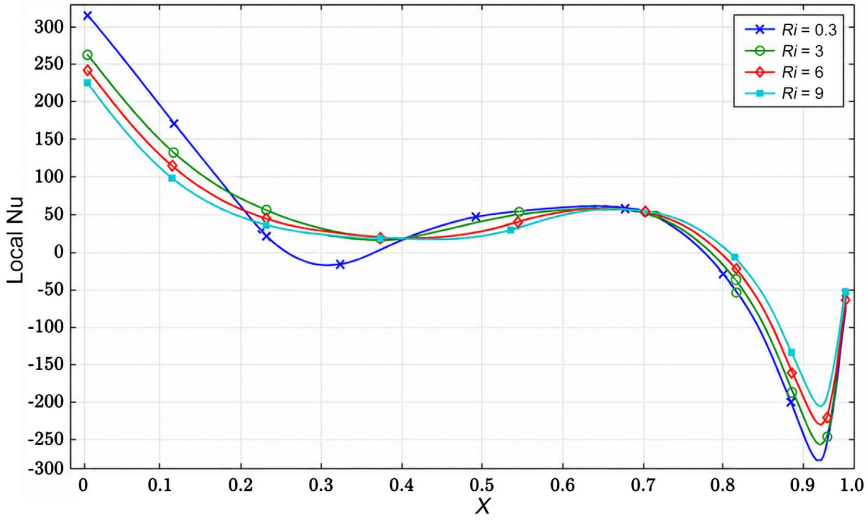

Figure 9. Effect of Local Nusselt for Ri along the line $y = 0.6$, while $Ha = 50$, $Pr = 0.71$ and $Re = 2000$.

At low Richardson number ($Ri = 0.3$), the flow is dominated by forced convection due to the moving lid. A strong primary vortex occupies most of the cavity, with weak secondary vortices near the corners. The isotherms are significantly distorted and aligned with the flow direction, indicating strong convective heat transfer.

As Ri increases to intermediate values ($Ri = 3$ and 6), buoyancy effects become more pronounced. The flow structure transitions into a mixed convection regime, characterized by deformation of the primary vortex and the development of secondary recirculation zones. The isotherms begin to show increased vertical stratification, reflecting the growing influence of thermal buoyancy.

At higher Richardson number ($Ri = 9$), natural convection dominates the flow behavior. The flow structure becomes more symmetric, and multiple vortices emerge due to buoyancy-induced circulation. The isotherms exhibit a layered pattern, indicating reduced convective mixing and a shift toward conduction-dominated heat transfer.

The velocity profiles (Figure 7) show a gradual reduction in peak velocity with increasing Ri, reflecting the weakening influence of lid-driven motion. Meanwhile, the temperature profiles (Figure 8) indicate increased thermal stratification as Ri increases. The local Nusselt number (Figure 9) decreases with increasing Ri, suggesting a reduction in heat transfer rate due to diminished forced convection effects.

6.2. Effect of Hartmann Number (Ha)

Figures 10-13 present the impact of the Hartmann number (Ha = 50, 100, 300, and 500) on flow and thermal characteristics at $Ri = 6$, $Re = 1$, and $Pr = 0.71$. The Hartmann number quantifies the strength of the applied magnetic field and its associated Lorentz force.

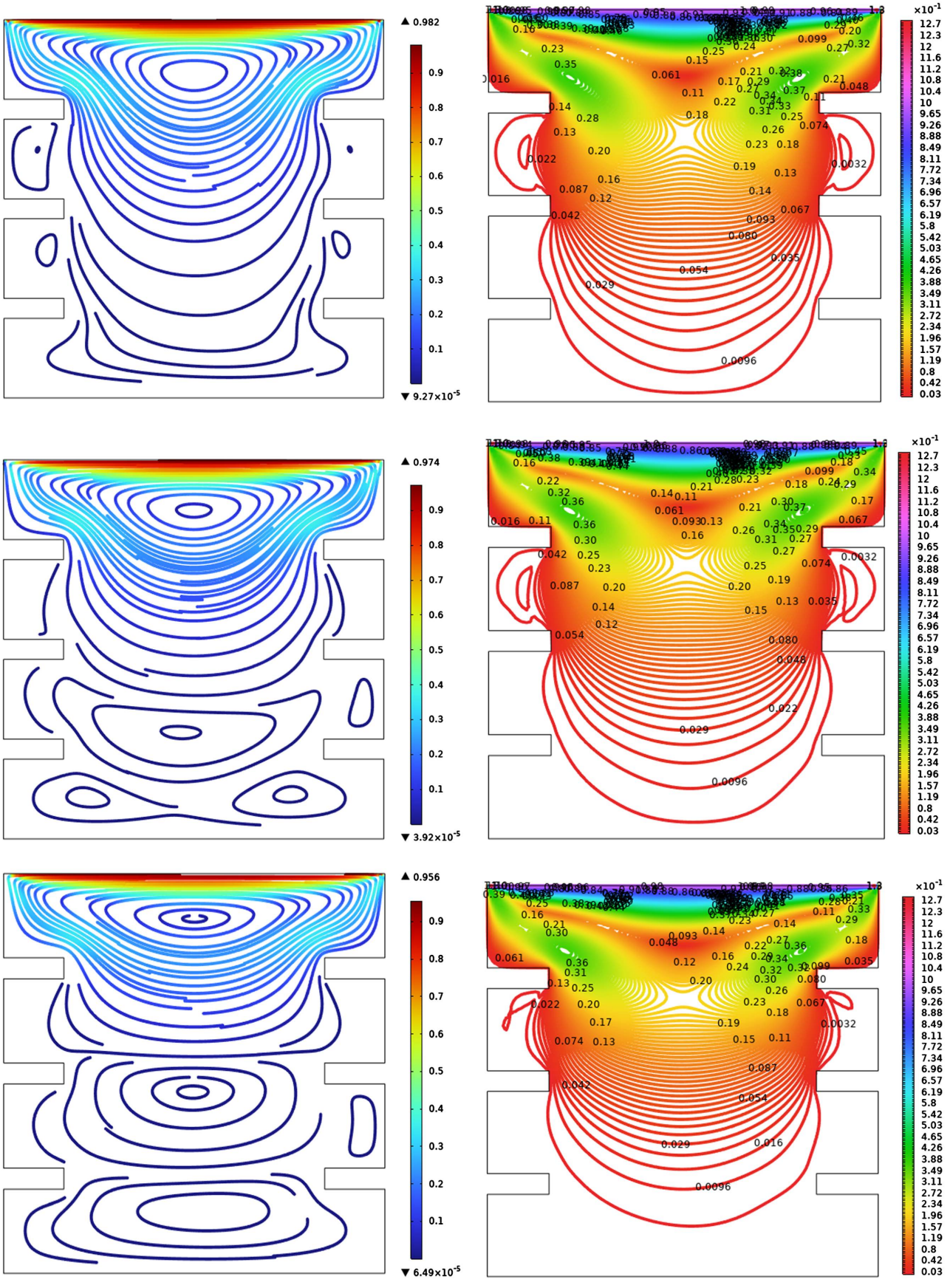
▲ 0.982
▼ 9.27×10⁻⁵
▲ 0.974
▼ 3.92×10⁻⁵
▲ 0.956
▼ 6.49×10⁻⁵
×10⁻¹

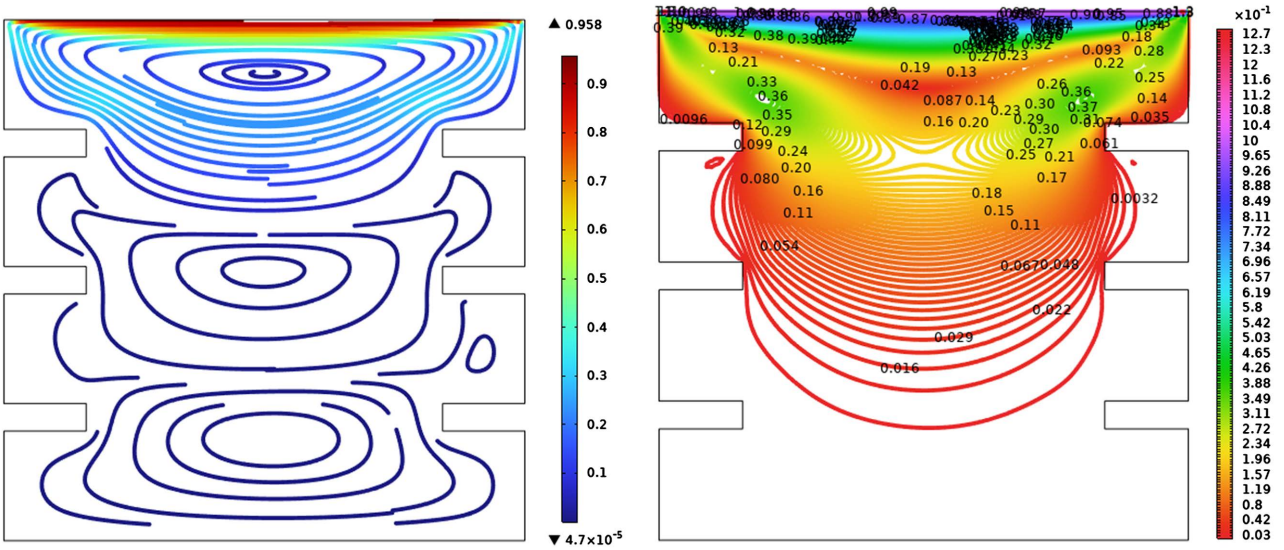

Figure 10. Streamlines (left column); Isotherms (right column) for $Ha = 50, 100, 300, 500$, while $Ri = 6$, $Pr = 0.71$ and $Re = 1$.

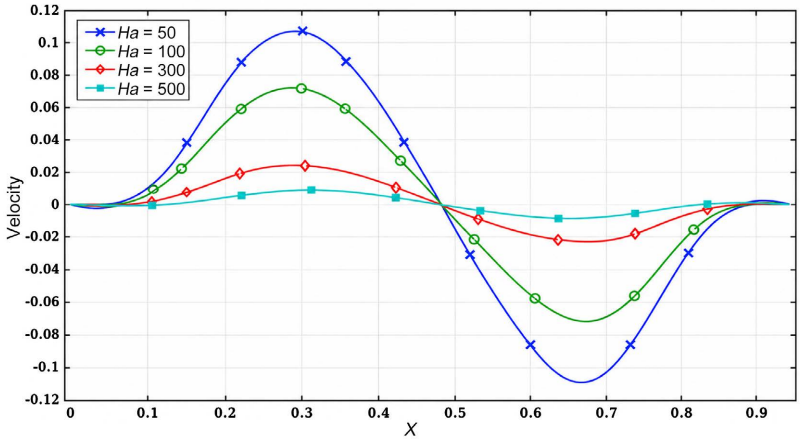

Figure 11. Effect of Velocity profile for Ha along the line $y = 0.6$, while $Ri = 6$, $Pr = 0.71$ and $Re = 1$.

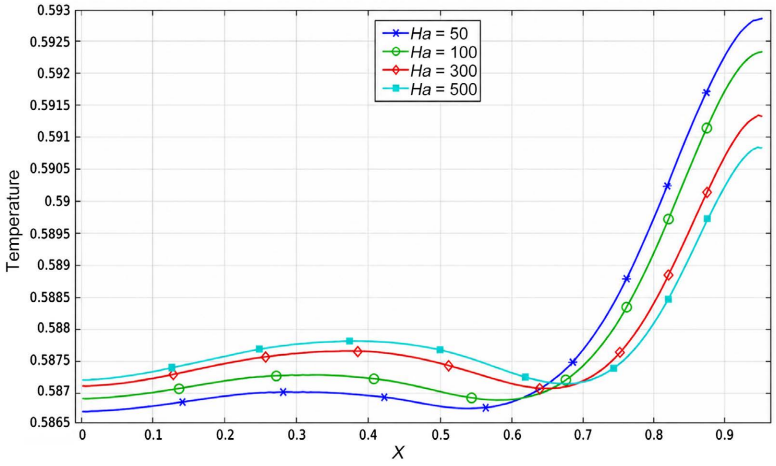

Figure 12. Effect of Temperature profile for Ha along the line $y = 0.6$, while $Ri = 6$, $Pr = 0.71$ and $Re = 1$.

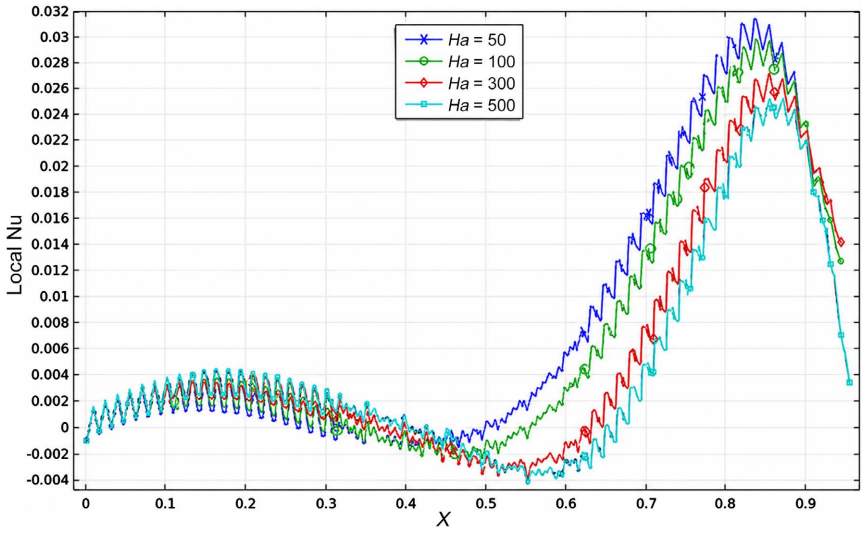

Figure 13. Effect of Local Nusselt for *Ha* along the line $y = 0.6$, while $Ri = 6$, $Pr = 0.71$ and $Re = 1$.

At low Hartmann number ($Ha = 50$), the magnetic field has a moderate influence on the flow. The fluid motion remains relatively strong, with a well-defined circulation pattern. The isotherms are slightly distorted, indicating the presence of convective heat transfer.

As *Ha* increases to 100 and 300, the Lorentz force significantly suppresses fluid motion. The primary vortex weakens, and the velocity magnitude decreases throughout the cavity. The flow becomes more stable and less oscillatory. Correspondingly, the isotherms become smoother and more parallel, indicating a transition toward conduction-dominated heat transfer.

At very high Hartmann number ($Ha = 500$), the flow is strongly damped, and convective effects are nearly eliminated. The fluid motion becomes negligible, and heat transfer occurs primarily through conduction. The isotherms exhibit a nearly linear distribution between the hot and cold walls.

The velocity profiles (**Figure 11**) confirm a substantial reduction in flow intensity with increasing *Ha*. Similarly, the temperature profiles (**Figure 12**) demonstrate reduced thermal gradients near the walls due to suppressed convection. The local Nusselt number (**Figure 13**) decreases significantly with increasing *Ha*, indicating a deterioration in heat transfer performance under strong magnetic fields.

6.3. Combined Effects of Magnetic Field and Buoyancy

The interaction between buoyancy forces (*Ri*) and magnetic effects (*Ha*) plays a crucial role in determining the overall transfer characteristics. While increasing *Ri* enhances natural convection and promotes fluid circulation, increasing *Ha* introduces a damping effect that suppresses motion.

At moderate *Ri* and low *Ha*, mixed convection is most effective, resulting in enhanced heat transfer due to the combined influence of shear and buoyancy

forces. However, at high *Ha*, even strong buoyancy forces are unable to overcome magnetic damping, leading to reduced convective transport.

7. Conclusions

The results demonstrate that heat transfer in the cavity is governed by a complex interplay of forced convection, natural convection, magnetic damping, and internal heat generation. Key observations include:

- Increasing **Richardson number (*Ri*)** shifts the regime from forced to natural convection, reducing heat transfer efficiency.
- Increasing **Hartmann number (*Ha*)** suppresses fluid motion and significantly reduces convective heat transfer.
- Optimal heat transfer occurs under **moderate *Ri* and low *Ha***, where mixed convection is strongest.

Conflicts of Interest

The authors declare no conflicts of interest regarding the publication of this paper.

References

[1] Oztop, H.F. and Dagtekin, I. (2004) Mixed Convection in Two-Sided Lid-Driven Differentially Heated Square Cavity. *International Journal of Heat and Mass Transfer*, **47**, 1761-1769. https://doi.org/10.1016/j.ijheatmasstransfer.2003.10.016

[2] Rahman, M.M.M. and Alim, M.A.A. (2010) MHD Mixed Convection Flow in a Vertical Lid-Driven Square Enclosure Including a Heat Conducting Horizontal Circular Cylinder with Joule Heating. *Nonlinear Analysis*: *Modelling and Control*, **15**, 199-211. https://doi.org/10.15388/na.2010.15.2.14354

[3] Jani, S., Mahmoodi, M. and Amini, M. (2013) Magnetohydrodynamic Free Convection in a Square Cavity Heated from Below and Cooled from Other Walls. *International Journal of Mechanical and Mechatronics Engineering*, **7**, 750-755.

[4] Hussein, A.K., Rout, S.K., Fathinia, F., Chand, R. and Mohammed, H.A. (2015) Natural Convection in a Triangular Top-Wall Enclosure with a Solid Strip. *Journal of Engineering Science and Technology*, **10**, 1326-1341.

[5] Rabbi, K.M., Saha, S., Mojumder, S., Rahman, M.M., Saidur, R. and Ibrahim, T.A. (2016) Numerical Investigation of Pure Mixed Convection in a Ferrofluid-Filled Lid-Driven Cavity for Different Heater Configurations. *Alexandria Engineering Journal*, **55**, 127-139. https://doi.org/10.1016/j.aej.2015.12.021

[6] Alam, M.S., Alim, M.A. and Mollah, M.S.H. (2017) Mixed Magneto Convection in a Lid Driven Square Enclosure with a Sinusoidal Vertical Wall and Joule Heating. *Procedia Engineering*, **194**, 463-470. https://doi.org/10.1016/j.proeng.2017.08.172

[7] Alam, M.S., Mollah, M.S.H., Alim, M.A. and Kabir, M.K.H. (2017) Finite Element Analysis of MHD Natural Convection in a Rectangular Cavity with a Partially Heated wall. *Engineering and Applied Sciences*, 2, 53-58.

[8] Alam, M.S., Mollah, M.S.H., Alim, M.A., Ali, M.M. and Munshi, M.J.H. (2019) Effect of Rayleigh Number Magneto-Convection in a Lid Driven Square Cavity with a Sinusoidal Wall. *AIP Conference Proceedings*, **2121**, Article 030021. https://doi.org/10.1063/1.5115866

[9] Munshi, M.J.H., Mostafa, G., Munsi, A.B.S.M. and Waliullah, M. (2018) Hydrody-

namic Mixed Convection in a Lid-Driven Hexagonal Cavity with Corner Heater. *American Journal of Computational Mathematics*, **8**, 245-258. https://doi.org/10.4236/ajcm.2018.83020

[10] Chamkha, A., Selimefendigil, F. and Oztop, H. (2018) MHD Mixed Convection and Entropy Generation in a Lid-Driven Triangular Cavity for Various Electrical Conductivity Models. *Entropy*, **20**, Article 903. https://doi.org/10.3390/e20120903

[11] Chowdhury, K. and Alim, A. (2019) MHD Mixed Convection Flow in a Lid Driven Enclosure with a Sinusoidal Wavy Wall and a Heated Circular Body. *International Journal of Fluid Mechanics & Thermal Sciences*, **5**, Article 102. https://doi.org/10.11648/j.ijfmts.20190504.13

[12] Haque, M.R., Alim, M.A., Alam, M.M. and Alam, M.S. (2019) Magnetohydrodynamic Free Convection in a Rectangular Enclosure with Three Square Heated Blocks. *International Journal of Theoretical and Applied Mathematics*, **5**, 74-82.

[13] Fayz-Al-Asad, M., Hossain, M.A. and Sarker, M.M.A. (2019) Numerical Investigation of MHD Mixed Convection Heat Transfer Having Vertical Fin in a Lid-Driven Square Cavity. *AIP Conference Proceedings*, **2121**, Article 030023. https://doi.org/10.1063/1.5115868

[14] Bakar, N.A., Roslan, R., Kamalrulzaman, M. and Akhir, M. (2020) Effects of Internal Heat Generation or Absorption on Mixed Convection in a Lid-Driven Rectangular Cavity Using the Finite Volume Method. *CFD Letters*, **12**, 38-54.

[15] Farahani, S.D., Amiri, M., Majd, B.K. and Mosavi, A. (2021) Effect of Magnetic Field on Heat Transfer from a Channel: Nanofluid Flow and Porous Layer Arrangement. *Case Studies in Thermal Engineering*, **28**, Article 101675. https://doi.org/10.1016/j.csite.2021.101675

[16] Runa, A.A., Alim, M.A., Alam, M.S. and Kabir, K.H. (2022) Finite Element Analysis of Magnetohydrodynamic Natural Convection within Semi-Circular Top Enclosure with Triangular Obstacles. *American Journal of Computational Mathematics*, **12**, 33-43. https://doi.org/10.4236/ajcm.2022.121004

[17] Keya, S.T., Yeasmin, S., Rahman, M.M., Karim, M.F. and Amin, M.R. (2022) Mixed Convection Heat Transfer in a Lid-Driven Enclosure with a Double-Pipe Heat Exchanger. *International Journal of Thermofluids*, **13**, Article 100131. https://doi.org/10.1016/j.ijft.2021.100131

[18] Mahmuda Maya, M.U., Alam, M.N. and Refaie Ali, A. (2023) Influence of Magnetic Field on MHD Mixed Convection in Lid-Driven Cavity with Heated Wavy Bottom Surface. *Scientific Reports*, **13**, Article No. 18959. https://doi.org/10.1038/s41598-023-45707-x

[19] Ali, M.Y., Islam, S., Alim, M.A., Biplob, R.A. and Islam, M.Z. (2024) Numerical Investigation of MHD Mixed Convection in an Octagonal Heat Exchanger Containing Hybrid Nanofluid. *Heliyon*, **10**, e37162. https://doi.org/10.1016/j.heliyon.2024.e37162

[20] Sarker, S.P.K. and Alam, M.M. (2025) Numerical Study of Heat Transfer in a Nanofluid-Filled Trapezoidal Enclosure with Star-Shaped Heat Sources under Magnetic Field. *Open Journal of Fluid Dynamics*, **15**, 136-157. https://doi.org/10.4236/ojfd.2025.153009

[21] Theeb, M.A., Abdulkadhim, A., Hamza, N.H., Al-Dawody, M.F., Sheremet, M. and Kadhem, W.J. (2025) Hybrid Nanofluid Mixed Convection in a Lid-Driven Wavy Cavity with Internal Heated Plate. *Results in Surfaces and Interfaces*, **18**, Article 100469. https://doi.org/10.1016/j.rsurfi.2025.100469